

Tweaking the spin-wave dispersion and suppressing the incommensurate phase in LiNiPO_4 by iron substitution

Jiying Li^{1,2,3}, Thomas B. S. Jensen⁴, Niels. H. Andersen⁴, Jerel L. Zarestky¹, R.

William McCallum⁵, Jae-Ho Chung⁶, Jeffrey W. Lynn², and David Vaknin^{1*}

¹Ames Laboratory and Department of Physics and Astronomy, Iowa State University, Ames, Iowa 50011

²NIST Center for Neutron Research, National Institute of Standards and Technology, Gaithersburg, MD 20899

³Department of Materials Science and Engineering,

University of Maryland, College Park, MD 20742

⁴Materials Research Division, Risø DTU, Technical University of Denmark, DK-4000 Roskilde, Denmark

⁵Ames Laboratory and Department of Materials Science and Engineering, Iowa State University, Ames, Iowa 50011 and

⁶Department of Physics, Korea University, Seoul 136-713 Korea

(Dated: November 8, 2018)

Elastic and inelastic neutron scattering studies of $\text{Li}(\text{Ni}_{1-x}\text{Fe}_x)\text{PO}_4$ single crystals reveal anomalous spin-wave dispersions along the crystallographic direction parallel to the characteristic wave vector of the magnetic incommensurate phase. The anomalous spin-wave dispersion (*magnetic soft mode*) indicates the instability of the Ising-like ground state that eventually evolves into the incommensurate phase as the temperature is raised. The pure LiNiPO_4 system ($x = 0$), undergoes a first-order magnetic phase transition from a long-range incommensurate phase to an antiferromagnetic ground state at $T_N = 20.8$ K. At 20% Fe concentrations, although the AFM ground state is to a large extent preserved as that of the pure system, the phase transition is second-order, and the incommensurate phase is completely suppressed. Analysis of the dispersion curves using a Heisenberg spin Hamiltonian that includes inter- and in-plane nearest and next-nearest neighbor couplings reveals frustration due to strong competing interactions between nearest- and a next-nearest neighbor site, consistent with the observed incommensurate structure. The Fe substitution only slightly lowers the extent of the frustration, sufficient to suppress the IC phase. An energy gap in the dispersion curves gradually decreases with the increase of Fe content from ~ 2 meV for the pure system ($x = 0$) to ~ 0.9 meV for $x = 0.2$.

PACS numbers: 75.25.+z, 75.50.Ee, 78.20.Ls

I. INTRODUCTION

Spontaneously occurring incommensurate (IC) structures can be classified into two general categories. The first group consists of systems for which the IC phase is the ground state, and the second group encompasses systems for which the IC phase manifests itself as an intermediate state between a commensurate ground state and a highly symmetric phase at higher temperatures[1, 2, 3]. Systems with incompatible interactions among nearest and next nearest neighbors that may lead to *geometrical frustration*, in general belong to the first group settling into an IC ground state[1]. Similarly, nearest-neighbors frustrations brought about by off-diagonal Dzyaloshinskii-Moriya type interactions, that compete with the isotropic interactions, can also give rise to IC ground states[4]. Magnetic systems consisting of interacting localized moments, such as MnSi [5], FeGe [6], NiBr_2 [7], $\text{Ba}_2\text{Cu}_2\text{Ge}_2\text{O}_7$ [8], CuB_2O_4 [9], LiCuVO_4 [10], and CdCr_2O_4 [11] are typical examples of the first group. On the other hand, the intermediate IC phases are in general electronically driven by instabilities due to the incompatibility in the interactions of a collective mode (phonon) and conduction electrons at the Fermi sur-

face. These structurally modulated phases are generally observed in metallic systems as charge density waves[12, 13], or martensitic transitions in alloys[14, 15], and occur at intermediate temperatures between a disordered state at high temperatures and a highly symmetric ground state at low temperatures[3]. Systems belonging to this second group possess a few distinct characteristics: 1) they undergo a first-order commensurate-incommensurate (C-IC) phase transition, 2) they give rise to strong diffuse scattering above and below the C-IC transition 3) they exhibit anomalies in their phonon dispersion curves that signal the emergence of the IC phase. A typical phonon anomaly appears as a minimum, or a dip, in the dispersion curve, commonly referred to as a *soft-mode*, at a wave-vector that defines the propagation vector and the shortest wavelength of the IC modulation. Due to the first-order nature of the C-IC transition, phonons are not well defined close to the transition, thus the whole dispersion curve, including the *soft mode*, abruptly disappears near the transition, and in turn, a *frozen phonon* sets in giving rise to a single peak at energy $\omega \approx 0$. The *frozen phonon*, realized as an elastic or quasi-elastic peak at and around the wavevector defining the IC structure, is identified with the IC structure.

An intriguing IC magnetic phase, with features that characterize the second group, has been found recently in the magnetoelectric crystal LiNiPO_4 . The IC phase occurs over a narrow range of intermediate temperatures

*electronic mail: vaknin@ameslab.gov

between an antiferromagnetic (AFM) ground state and a high temperature paramagnetic phase[16]. Here, it was found that LiNiPO₄ undergoes a first order transition from the antiferromagnetic ground state to a long-range IC order at a Néel temperature, $T_N = 20.8$ K ($T_N \equiv T_{C-IC}$). As the temperature is increased, a second-order phase transition from long-range incommensurate magnetic order to the paramagnetic state occurs at $T_{IC} = 21.7$ K[16, 17]. The incommensurate spin correlations gradually weaken and the spins are essentially uncorrelated by $T \approx 35$ K. In addition to exhibiting a first order C-IC phase transition, strong diffuse scattering below and above the transition has also been reported[16]. This unusual magnetic intermediate IC phase has characteristics that classify it with the second group mentioned above, however, it should be noted that LiNiPO₄ is an insulator (with an energy gap of approximately 1 eV), thus the IC phase cannot be induced by interaction with conduction electrons.

A recent neutron scattering study[18] investigated the spin dynamics of pure LiNiPO₄ to determine the spin Hamiltonian and identify other features that characterize the aforementioned second group of IC systems, particularly looking for a *soft-magnetic mode*, the analog of the *soft mode* in structurally IC systems. An unusual minimum in the spin-wave dispersions in the AFM commensurate ground state was observed at the modulation vector of the IC phase, and was explained as the precursor of the C-IC phase transition that originates from a trade off between competing Heisenberg interactions of nearest and next-nearest neighboring Ni²⁺ ions and an extra *lock-in* energy at lower temperatures originating from the strong single ion anisotropies found in the system [18]. We have recently reported on the spin dynamics and magnetic properties of the isostructural LiFePO₄, LiCoPO₄ and LiMnPO₄ systems and found no evidence for an IC phase and no anomalous spin-wave dispersions [19, 20, 21]. In the present study we have substituted Fe for Ni to form LiNi_{1-x}Fe_xPO₄ single crystals with up to $x = 0.2$ to compare with the magnetic behavior of the parent material and shed further light on the IC phase in LiNiPO₄. Our studies show that, up to a substitution level greater than ~ 0.15 iron, the IC phase is still present, and only at higher Fe concentrations does it disappear completely[22]. We report herein the spin dynamics of LiNi_{0.8}Fe_{0.2}PO₄, that do not show evidence for the IC magnetic structure, and compare the results with measurements of pure LiNiPO₄.

LiNiPO₄ is an insulator belonging to the olivine family of lithium orthophosphates LiMPO₄ ($M = \text{Mn, Fe, Co, and Ni}$) with space group $Pnma$ [23]. All members of this family were found to be antiferromagnets with the same magnetic structure differing only in the spin-direction[24, 25, 26], however a recent single crystal study of LiNiPO₄ revealed that the magnetic spins are not co-linear in the AFM ground state but are slightly canted within the *ac*-plane [27]. Neutron scattering studies demonstrated that LiMPO₄ ($M = \text{Ni, Co, Mn}$) ex-

hibit properties between two-dimensional (2D) and three-dimensional (3D) with an interlayer coupling that is stronger relative to the coupling found in the cuprates, for instance[19, 20, 21, 28, 29]. These insulators also exhibit strong linear magnetoelectric (ME) effects, with the observed ME tensor components, α_{xz}, α_{zx} , for LiNiPO₄, in agreement with the antiferromagnetic point groups $mm'm$, but with some anomalies[30, 31, 32]. In particular, the ME effect measurements of LiNiPO₄ as a function of temperature reveal a first-order AFM transition, and an unusual decrease of the ME coefficient at temperatures below a maximum close to T_N [16, 30]. Recently, a microscopic model combining super-exchange and Dzyaloshinsky-Moriya interactions with elastic displacements of exchange mediating ions has accurately explained the temperature dependence of the ME coefficients in LiNiPO₄ [27]. The model shows that the sharp decrease of α_{xz} and α_{zx} as a function of temperature is intimately connected to the first-order nature of the C-IC phase transition in LiNiPO₄. By contrast, the isostructural materials, LiCoPO₄, LiFePO₄, and LiMnPO₄, all exhibit a continuous change of the ME coefficients [31] reflecting the second-order nature of their magnetic phase transition from a commensurate AFM state to the paramagnetic state. Magnetic susceptibility studies of polycrystalline LiNiPO₄ showed a significant deviation from the Curie-Weiss law in a temperature range much higher than T_N , and neutron scattering from the same polycrystalline sample gave rise to diffuse scattering at the nominal position of the AFM Bragg reflection up to $T \approx 2T_N$ [28]. Recent magnetic susceptibility measurements of single crystal LiNiPO₄ showed two features, one at $T_N = 20.8$ K and one at $T_{IC} = 21.7$ K associated with an AFM transition and an intermediate IC phase [17], in agreement with the observed neutron diffraction data [16].

II. EXPERIMENTAL DETAILS

LiNiPO₄ single crystals were grown by the standard flux growth method (LiCl was used as the flux) from a stoichiometric mixture of high purity NiCl₂(99.999%) and Li₃PO₄ (99.999%)[33]. To prepare LiNi_{0.8}Fe_{0.2}PO₄, the Fe substitution was introduced by adding FeCl₂(99.999%) to the flux at a molar ratio of 1:4 to NiCl₂. The composition of Li(Ni_{0.8}Fe_{0.2})PO₄ single crystals were confirmed by chemical analysis. X-ray diffraction and GSAS refinement show that Li(Ni_{0.8}Fe_{0.2})PO₄ has the same crystal structure and symmetry group as pure LiNiPO₄.

The magnetic susceptibility measurements were performed on a superconducting quantum interference device (SQUID) magnetometer. The single crystals used for magnetic property measurements were oriented using Laue back scattering x-ray diffraction. For the different measurements, the single crystals were glued to a plastic straw with the specified axis parallel to the applied

magnetic fields with error less than 5° .

Elastic and inelastic neutron scattering studies of LiNiPO_4 were performed on the HB1A spectrometer at High Flux Isotope Reactor (HFIR) at Oak Ridge National Laboratory. A monochromatic neutron beam of wavelength $\lambda = 2.37 \text{ \AA}$ (14.61 meV , $k_o = 2\pi/\lambda = 2.66 \text{ \AA}^{-1}$) was selected by a double monochromator system, using the (002) Bragg reflection of highly oriented (mosaicity 0.3 deg) pyrolytic graphite (HOPG) crystals. The collimating configuration 40'-40'-Sample-34'-68' was used throughout the experiments, yielding an average energy resolution of $\approx 1 \text{ meV}$. Two sets of HOPG crystals, located between and after the monochromator crystals, were used as filters removing the $\lambda/2$ component from the incident beam to better than one part in 10^4 . Elastic neutron scattering from $\text{Li}(\text{Ni}_{0.8}\text{Fe}_{0.2})\text{PO}_4$ single crystals was measured on the HB1A spectrometer, and the inelastic neutron scattering was measured on the Spin Polarized Inelastic Neutron Spectrometer (SPINS) at the NIST Center for Neutron Research (NCNR) using a fixed final energy of 5 meV . The collimating configuration 80'-Sample-Be filter-80' was used for these measurements yielding an energy resolution $\approx 0.2 \text{ meV}$.

III. EXPERIMENTAL RESULTS

A. Magnetic Susceptibility

Magnetic susceptibility measurements of LiNiPO_4 and $\text{Li}(\text{Ni}_{0.8}\text{Fe}_{0.2})\text{PO}_4$ single crystals along the easy c -axis are shown in Fig. 1 (a). The measured magnetic susceptibilities of the two systems are different in two respects. First, the absolute value of the susceptibility in Fig. 1 (a) is larger for the iron substituted sample, indicating the presence of uncompensated paramagnetic sites, due to the random distribution of iron spins ($S = 2$) with a moment that is different than that of Ni^{+2} ($S = 1$). We note that susceptibility measurements under field- or zero-field cooling indicate subtle spin-glass properties[22]. Second, large differences are identified in the derivatives of the susceptibilities with respect to temperature, as shown in Fig. 1 (b). In agreement with previous measurements of LiNiPO_4 [17], the main AFM-IC transition has the characteristics of a first order transition, and the anomaly associated with the transition from the long-range IC structure to the paramagnetic state at $T_{IC} = 21.7 \text{ K}$ is in good agreement with the neutron diffraction studies[16]. By contrast the Fe substituted ($x = 0.2$) crystal has only one smooth feature characteristic of a second order phase transition with no indication of a secondary transition. We therefore conclude that whereas the Fe substitution maintains the AFM ground state for all $x \lesssim 0.2$ it does not modify the nature of the transition and does not eliminate the IC long-range order up to a substitution level of $x \sim 0.2$.

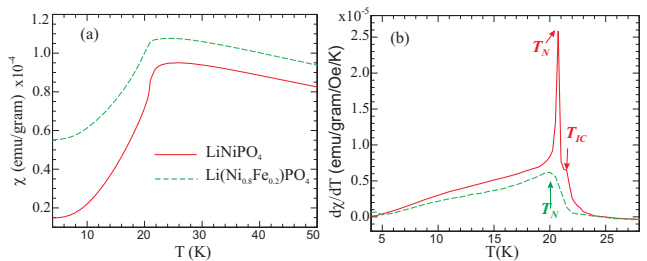


FIG. 1: (color online) (a) Susceptibility measurements of LiNiPO_4 (solid line) and $\text{Li}(\text{Ni}_{0.8}\text{Fe}_{0.2})\text{NiPO}_4$ (dashed line). (b) The respective derivatives of the susceptibilities with respect to temperature, showing the two features due to the transitions to IC and AFM in pure LiNiPO_4 and a single broad feature (second order transition) in $\text{Li}(\text{Ni}_{0.8}\text{Fe}_{0.2})\text{PO}_4$

B. Elastic Neutron Scattering

Neutron diffraction measurements confirm the orthorhombic structure of both the pure and the Fe substituted samples. For pure LiNiPO_4 we find the following room temperature lattice parameters of $a = 10.030$, $b = 5.847$, and $c = 4.677 \text{ \AA}$ and for $\text{Li}(\text{Ni}_{0.8}\text{Fe}_{0.2})\text{PO}_4$ we find $a = 10.057$, $b = 5.881$, and $c = 4.672 \text{ \AA}$ at 10 K . For the $x = 0.2$ sample, we identified a weak nuclear peak (at room temperature), not identified in the X-ray diffraction of the powder, at the (010) that may indicate a small structural distortion along the b -axis. In general, elastic neutron scattering and magnetic susceptibility measurements of the Fe substituted $\text{Li}(\text{Ni}_{1-x}\text{Fe}_x)\text{PO}_4$ crystals show the low-temperature ground states of these systems are antiferromagnetic with a magnetic arrangement similar to that found in pure LiNiPO_4 .

The magnetic spins in LiNiPO_4 are primarily directed along the c -axis in the AFM ground state, but are slightly canted with a small component along the a -axis. As the Fe concentration is increased, up to at least $x \approx 0.2$, the Néel temperature changes slightly but the nature of the order parameter changes more dramatically. Figure 2 shows the temperature dependencies of the magnetic order parameters for LiNiPO_4 and $\text{Li}(\text{Ni}_{0.8}\text{Fe}_{0.2})\text{PO}_4$ as measured on the (010) magnetic peak. As previously discussed[16], LiNiPO_4 undergoes a first order magnetic phase transition from commensurate AFM ground state (labeled A in Fig. 2) to a long-range incommensurate structure at $T_N = 20.8 \text{ K}$, and subsequently to the paramagnetic state at $T_{IC} \approx 21.7 \text{ K}$ by a second-order phase transition. The incommensurate spin correlations are gradually lost by a temperature between 34 K to 40 K . In contrast, the transition from the AFM to the paramagnetic phase in $\text{Li}(\text{Ni}_{0.8}\text{Fe}_{0.2})\text{PO}_4$ is continuous, i.e., it is a second-order phase transition to the paramagnetic phase with no clear evidence for any intermediate magnetic phases. The temperature dependent order-parameter for $\text{Li}(\text{Ni}_{0.8}\text{Fe}_{0.2})\text{PO}_4$, shown in Fig. 2, was fit to a power-law function (solid line) yielding a transition temperature $T_N = 20.6 \pm 0.2 \text{ K}$ and a critical exponent $\beta = 0.33 \pm 0.03$.

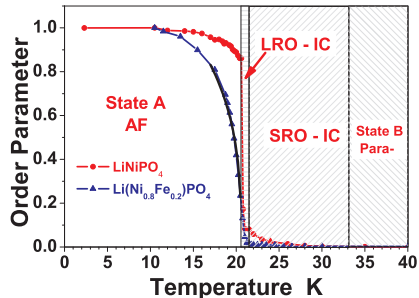


FIG. 2: (color online) Magnetic order parameter of pure LiNiPO_4 and $\text{Li}(\text{Ni}_{0.8}\text{Fe}_{0.2})\text{PO}_4$ versus temperature. LiNiPO_4 undergoes a first order phase-transition from antiferromagnetic ground state to long-range incommensurate structure at $T_N = 20.8$ K, and at $T_{IC} \approx 21.7$ K the IC structure transforms to the paramagnetic state. The incommensurate spin correlations become negligible at about 35 to 40 K. By comparison, $\text{Li}(\text{Ni}_{0.8}\text{Fe}_{0.2})\text{PO}_4$ transforms from the collinear ground state to the paramagnetic state by a second order phase transition at $T_N = 20.6$ K. The labeled temperature regions refer to phases of pure LiNiPO_4 .

Figure 3 shows scans along the $(0k0)$ direction for the pure and $x = 0.2$ samples above the Néel temperature. Whereas these scans for LiNiPO_4 above 20.8 K show two satellite peaks due to the IC phase, with intensities, peak-shapes, and wave-vectors that are strongly temperature dependent, no similar peaks along the $(0k0)$ direction or along any other principal direction were detected for $\text{Li}(\text{Ni}_{0.8}\text{Fe}_{0.2})\text{PO}_4$.

C. Inelastic Neutron Scattering

Figure 4(a) shows constant-Q energy scans of spin-waves propagating along $(0q0)$ for LiNiPO_4 at 10 K measured on the HB1A spectrometer at HFIR (energy resolu-

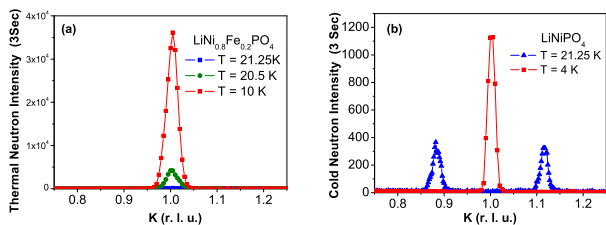


FIG. 3: (color online) Longitudinal scans along the $(0k0)$ direction for (a) $\text{Li}(\text{Ni}_{0.8}\text{Fe}_{0.2})\text{PO}_4$ and (b) LiNiPO_4 . Above the Néel temperature no satellite peaks, due to the long-range incommensurate structure, were observed for $\text{LiNi}_{0.8}\text{Fe}_{0.2}\text{PO}_4$ in the temperature range between 18 K to 22 K with 0.25 K temperature steps. The error bars in this paper are statistical in origin and represent one standard deviation. (r.l.u, stands for reciprocal lattice units, for example for the $(0q0)$ direction q is normalized to $b^* = 2\pi/b$.)

tion ≈ 1 meV). Similar constant-Q energy scans obtained on the SPINS spectrometer at NCNR (energy resolution 0.2 meV at zero energy transfer) on $\text{Li}(\text{Ni}_{0.8}\text{Fe}_{0.2})\text{PO}_4$ at 4 K are shown in Fig. 4(b). Each constant-Q scan was fit to a Gaussian profile (including a constant background) shown as solid lines. Using this analysis, the spin-wave dispersion curves along all the three principal directions, $(\xi00)$ $(0\xi0)$ and (00ξ) for both crystals were compiled in Fig. 5. The dispersion curves show an energy gap that decreases with iron substitution. A gap of $\Delta E \sim 1.9$ meV is observed for LiNiPO_4 compared with $\Delta E \sim 0.9$ meV for $\text{Li}(\text{Ni}_{0.8}\text{Fe}_{0.2})\text{PO}_4$. The dispersion curves along the propagation vector $(0q0)$ of the AFM structure are softer (lower in energy) than the curves along the other principal directions. In particular, it is even softer than inter-layer spin-waves, along the $(q00)$ direction, propagating perpendicular to the b - c planes. This behavior should be contrasted with the spin-waves of isostructural LiFePO_4 , where the dispersion along the $(0q0)$ direction[19] is stiffer than that along the $(q00)$. Most importantly, for small q 's the curve is almost flat, with a shallow minimum at $q \approx 0.1$, i.e., a *soft magnetic mode*, whereas for a simple gapless AFM systems the spin-wave dispersion is expected to be linear at small wave-vectors. We identify the anomalous spin-wave dispersion along $(0,q,0)$ direction with the *soft magnetic mode*.

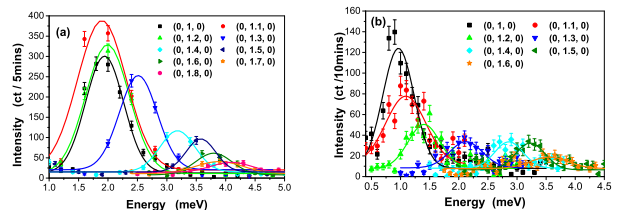


FIG. 4: (color online) (a) Constant-Q energy scans along the $(0q0)$ for a single crystal LiNiPO_4 at 10 K (b) and for $\text{Li}(\text{Ni}_{0.8}\text{Fe}_{0.2})\text{PO}_4$ at 4 K. The solid lines are Gaussian fits including constant background. All modes were measured from the (010) zone center.

The substitution of Fe in $\text{Li}(\text{Ni}_{1-x}\text{Fe}_x)\text{PO}_4$ modifies both the energy gap and the overall dispersion curves. In particular, the mode along the $(0q0)$ direction is modified and the shallow minimum is not observed, as shown in Fig. 4 for $\text{Li}(\text{Ni}_{0.8}\text{Fe}_{0.2})\text{PO}_4$. These modifications in the spin-wave dispersion, are not striking considering the fact that the IC phase is not present in this crystal. This may suggest that although the ingredients for the IC phase to occur are still present, namely competing interactions that lead to frustration, they are not sufficiently strong or coherent to stabilize an equilibrium IC phase above T_N .

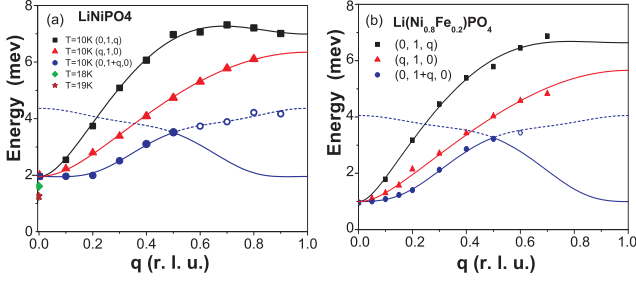


FIG. 5: (color online) Spin wave dispersion curves along the $(00q)$, $(0q0)$ and $(q00)$ directions at (a) 10 K for LiNiPO_4 , (b) at 4 K for $\text{Li}(\text{Ni}_{0.8}\text{Fe}_{0.2})\text{PO}_4$. The solid and dashed lines are fits using the spin-wave Eq. (2). The dotted line starting at the zone center indicates the spin wave optical branch.

IV. ANALYSIS AND DISCUSSION

A. Linear Spin-Wave Theory

To analyze the measured spin-wave data we follow the model of [18] using linear Holstein-Primakoff spin-wave theory [18, 34] to calculate the eigenvalues as a function of wavevectors. The interaction parameters determining the eigenvalues are then refined by a non-linear-least-square fit to the measured dispersion curves. LiNiPO_4 adopts the $Pnma$ symmetry group, in which Ni^{2+} ($S = 1$) ions occupy the centers of slightly distorted NiO_6 octahedra, and P ions are located at the centers of PO_4 tetrahedra. The NiO_6 octahedra are corner shared and cross-linked with the PO_4 tetrahedra forming a buckled two-dimensional plane normal to the a -axis. The atomic structure and definition of spin coupling, used in this study, are illustrated in Fig. 6. The small canting of the Ni^{2+} spins has a negligible influence on the spin wave model [18] so for simplicity we have assumed a ground state with spins pointing strictly along the c axis. The in-plane nearest-neighbor (NN) coupling (J_1) is mediated by an oxygen through a $\text{Ni}^{2+}\text{-O-Ni}^{2+}$ bond. The distances between the inplane NN are 3.806 \AA . There are two in-plane next-nearest-neighbors (NNN), with distances of 5.891 \AA and 4.705 \AA , with inplane couplings J_2 and J_3 , respectively. These NNN are linked via $\text{Ni}^{2+}\text{-O-P-O-Ni}^{2+}$ bond. For inter-layer coupling, we consider only the NN interactions J_4 and J_5 in adjacent layers (5.397 and 5.495 \AA apart, respectively). The exchange interaction between NN in adjacent layers is through phosphate tetrahedra. The spin-coupling via phosphate tetrahedra can be significant and cannot be ignored, as has been found for $\text{Li}_3\text{Fe}_2(\text{PO}_4)_3$ where all spins are coupled via phosphate tetrahedra [35]. In addition to the Heisenberg interactions, the spin Hamiltonian includes standard single-ion anisotropy terms $D_\xi(S^\xi)^2$ ($\xi = x, y, z$) as follows,

$$\mathcal{H} = \sum_{i,j} (J_{\{i,j\}} \mathbf{S}_i \cdot \mathbf{S}_j) + \sum_{i,\xi} D_\xi (S_i^\xi)^2, \quad (1)$$

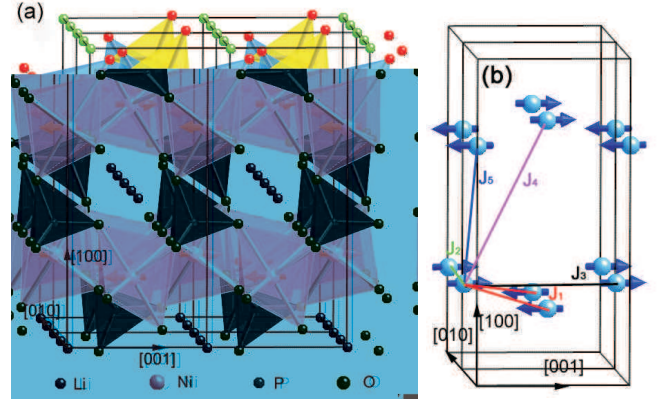


FIG. 6: (color online) (a) Atomic structure of LiNiPO_4 . The magnetic moments of Ni^{2+} are along c -axis in LiNiPO_4 . (b) Illustration of spin couplings in LiNiPO_4 . The same definitions of bonding are used in the spin wave Hamiltonian

where $D_{x,y,z}$ are the single ion anisotropies along the a , b and c axis respectively. Since the excitation spectrum is insensitive towards an overall shift in the ground state energy we define $D_z \equiv 0$ for simplicity. The magnon dispersion derived from Eq. (1) by linear spin-wave theory is given by Eq. (2).

$$\hbar\omega = \sqrt{A^2 - (B \pm C)^2}, \quad (2)$$

where,

$$A \equiv 4S(J_1 + J_5) - 2S[J_2(1 - \cos(\mathbf{q} \cdot \mathbf{r}_5)) + J_3(1 - \cos(\mathbf{q} \cdot \mathbf{r}_6)) + J_4(2 - \cos(\mathbf{q} \cdot \mathbf{r}_7) - \cos(\mathbf{q} \cdot \mathbf{r}_8))] + (S - 1/2)(D_x + D_y), \quad (3)$$

$$B \equiv (S - 1/2)(D_x - D_y), \quad (4)$$

$$C \equiv 2J_1S[\cos(\mathbf{q} \cdot \mathbf{r}_1) + \cos(\mathbf{q} \cdot \mathbf{r}_2)] + 2J_5S[\cos(\mathbf{q} \cdot \mathbf{r}_3) + \cos(\mathbf{q} \cdot \mathbf{r}_4)], \quad (5)$$

and \mathbf{r}_i denotes a vector to a NN and NNN, $\mathbf{r}_1 = (0, b/2, c/2)$; $\mathbf{r}_2 = (0, b/2, -c/2)$; $\mathbf{r}_3 = (a/2, b/2, 0)$; $\mathbf{r}_4 = (a/2, -b/2, 0)$; $\mathbf{r}_5 = (0, b, 0)$; $\mathbf{r}_6 = (0, 0, c)$; $\mathbf{r}_7 = (a/2, 0, c/2)$; $\mathbf{r}_8 = (a/2, 0, -c/2)$. In our model, the calculated spin waves have two non-degenerate branches (denoted by the \pm sign in Eq. 2) as a result of the different anisotropies along the x , y and z direction.

The energy gaps at $\mathbf{q} = 0$ for the two branches are

$$\Delta E = \sqrt{16S(S - 1/2)D_x(J_1 + J_5) + 4(S - 1/2)^2D_xD_y}, \quad (6)$$

for $(B - C)$ in equation 2 and

$$\Delta E = \sqrt{16S(S - 1/2)D_y(J_1 + J_5) + 4(S - 1/2)^2D_xD_y}, \quad (7)$$

for $(B + C)$. The equations show that the energy gaps depending on both the single-ion anisotropy terms and the exchange interactions.

$S = 1$ and $S = 1.2$ are used for LiNiPO_4 and $\text{Li}(\text{Ni}_{0.8}\text{Fe}_{0.2})\text{PO}_4$, respectively. The experimental data for LiNiPO_4 and for $\text{Li}(\text{Ni}_{0.8}\text{Fe}_{0.2})\text{PO}_4$ were simultaneously fit for the three principal directions by Eq. 2 using the (B - C) dispersion. The best fits, shown by solid lines in Fig. 5 were obtained by using the parameters listed in Table I. It is noted that the values given in Table I for pure LiNiPO_4 are consistent with those reported in Ref. 18. The dashed lines in Fig. 5 are the second mode of the spin wave calculated using (B + C) in Eq. 2 and the parameters listed in Table I. For the spin wave dispersion along the $(0, 1+q, 0)$ direction, several excitations for the second mode were measured. It is clearly shown in Table I that the inplane NN exchange J_1 is much larger than the inter-plane NN exchanges, J_4 and J_5 , consistent with the quasi-2D character of the system. The coupling constants also show that the NNN inplane coupling along the b -axis J_2 has the same sign as that of J_1 , implying competing interactions. In particular we find that J_2 , which couples spins along the b -axis, is significantly larger than J_3 that couples NNN along the c -axis. This is the direction along which the IC structure is realized. The single ion anisotropies, D_x and D_y , are both positive indicating that a c -axis magnetic moment is a favorable ground state, as observed experimentally. The Fe substitution systematically weakens all effective spin-couplings and the single ion anisotropies. Two non-degenerate branches of the spin wave dispersion have been observed at several scattering vectors in LiNiPO_4 using the high-flux thermal neutron triple axis IN8 at Institut Laue-Langevin (ILL) and were perfectly fit by the proposed spin-wave model [18].

TABLE I: Best fit exchange parameters and single ion anisotropies used to fit the dispersion curves in Fig. 5.

	LiNiPO_4	$\text{LiNi}_{0.8}\text{Fe}_{0.2}\text{PO}_4$
J_1	0.94(08)	0.88(15)
J_2	0.59(05)	0.44(04)
J_3	-0.11(05)	0.087(02)
J_4	-0.16(02)	-0.22(04)
J_5	0.26(02)	0.038(004)
D_x	0.34(06)	0.072(006)
D_y	1.92(01)	1.47(1)
D_z	0	0

V. SUMMARY

Model calculations of spin systems with competing interactions between NN and NNN have demonstrated that anomalous spin-waves, i.e., *soft-magnetic-mode* are possible for such frustrated systems [36, 37]. The spin couplings for the Fe substituted compound ($x = 0.2$) are slightly different than those of the pure one with sim-

ilar frustrations, but they do not lead to the IC phase. The realization of the IC phase as an intermediate state may be related to the energy gap compared to thermal energies at T_N . It is interesting to note that the energy gap observed in the dispersion curves of the pure system is very close to $k_B T_N$, i.e., $\Delta E \approx 1.9$ meV = 22 K. By contrast the energy gap in the Fe substituted system is much lower than the intrinsic T_N temperature $\Delta E \approx 0.9$ meV = 10 K. Thus, although the ingredients for the IC phase are present in the Fe substituted sample and give rise to diffuse scattering, they cannot stabilize the IC structure at any temperature. Another measure for the feasibility of an IC phase is the ratio of the competing in-plane couplings J_2/J_1 , for example. The reduction of the ratio from $J_2/J_1 \approx 0.63$ for LiNiPO_4 to $J_2/J_1 \approx 0.5$ for the Fe substituted system ($x = 0.2$) is sufficient to destabilize the IC phase. $\text{LiFePO}_4\text{LiFePO}_4$, with $J_2/J_1 \sim 0.4$, exhibits a second-order paramagnetic-AFM phase transition with no evidence for the IC magnetic structure at any temperature [19].

In summary, inelastic neutron scattering studies of LiNiPO_4 and $\text{Li}(\text{Ni}_{0.8}\text{Fe}_{0.2})\text{PO}_4$ show the spin-dynamics of these systems is anomalous. Whereas the anomaly in the pure material leads to an IC intermediate state, the reduced anomaly in the perturbed system with the substitution of Fe for Ni does not exhibit an IC magnetic structure. The spin wave dispersion curves for both systems were analyzed using the eigenvalues obtained from a Heisenberg-like spin Hamiltonian by linear spin wave theory. The spin couplings obtained indicate frustration between inplane NN and NNN, in particular along the direction that the IC structure is observed. Although Fe substitution does alter the ground state, and preserves the frustration to a lesser degree, it eliminates the IC phase altogether.

Acknowledgments

The work at Ames Laboratory was supported by the Department of Energy, Office of Basic Energy Sciences under contract number DE-AC02-07CH11358. This work was supported (in part) under the auspices of the United States Department of Energy. The HFIR Center for Neutron Scattering is a national user facility funded by the United States Department of Energy, Office of Basic Energy Sciences- Materials Science, under Contract No. DE-AC05-00OR22725 with UT-Battelle, LLC. We acknowledge the support of the National Institute of Standards and Technology, U.S. Department of Commerce, in providing the neutron research facilities used in this work which is supported by the National Science Foundation under Agreement No. DMR-0454672. JHC is supported by the KOSEF grant No. R01-2008-000-10787-0 funded by the Korean government (MEST).

-
- [1] P. Bak, Rep. Prog. Phys. **45**, 587 (1982).
- [2] T. Tsakalacos, Editor *Modulated Structure Materials*, Martinus Nijhoff Publishers, Dordrecht (1984).
- [3] J. F. Mitchell and J. K. Burdett, J. Chem. Phys. **102**, 6762 (1995).
- [4] I. E. Dzyaloshinskii, J. Exp. Theor. Phys. **46**, 1420 (1964).
- [5] T. Moriya, Phys. Rev. **120**, 91 (1960).
- [6] P. Bak and M. H. Jensen, J. Phys. C **13**, L881 (1980).
- [7] P. Day, M. W. Moore, T. E. Wood, D. McK. Paul, K. R. A. Ziebeck, L. P. Regnault, and J. Rossat-Mignod, Solid State Comm. **51**, 627 (1984).
- [8] A. Zheludev, S. Maslov, G. Shirane, I. Tsukada, T. Masuda, K. Uchinokura, I. Zaliznyak, R. Erwin, and L. P. Regnault, Phys. Rev. B **59**, 11432 (1999).
- [9] B. Roessli, J. Schefer, G. A. Petrakovskii, B. Ouladdiaf, M. Boehm, U. Staub, A. Vorotinov, and L. Bezmaternikh, Phys. Rev. Lett. **86**, 1885 (2001).
- [10] M. Enderle, C. Mukherjee, B. Fak, et. al., Europhys. Lett. **70**, 237 (2005).
- [11] J.-H. Chung, M. Matsuda, S. -H. Lee, K. Kakurai, H. Ueda, T. J. Sato, H. Takagi, K. -P. Hong, and S. Park, Phys. Rev. Lett. **95**, 247204 (2005).
- [12] D. E. Moncton, J. D. Axe, and F. J. DiSalvo Phys. Rev. Lett. **34**, 734 (1975).
- [13] A. H. Moudden, F. Denoyer, J. P. Benoit, and W. Fitzgerald, Solid State Communications **28**, 575 (1978).
- [14] R. J. Gooding, J. A. Krumhansl, Phys. Rev. B **39**, 1535 (1989).
- [15] Y. Noda, S. M. Shapiro, G. Shirane, Y. Yamada, and L. E. Tanner, Phys. Rev. B **42**, 10397 (1990).
- [16] D. Vaknin, J. L. Zarestky, J. -P. Rivera, and H. Schmid, Phys. Rev. Lett. **92**, 207201 (2004).
- [17] Yu. N. Kharchenko and N. F. Kharchenko, Low Temp. Phys. **29**, 579 (2003).
- [18] T. B. S. Jensen, N. B. Christensen, M. Kenzelmann, H. M. Rønnow, C. Niedermayer, N. H. Andersen, K. Lefmann, M. Jiménez-Ruiz, F. Demmel, J. Li, J. L. Zarestky, and D. Vaknin, Phys. Rev. B, **79**, 092413 (2009).
- [19] J. Li, V. O. Garlea, J. L. Zarestky, and D. Vaknin, Phys. Rev. B **73**, 024410 (2006).
- [20] W. Tian, J. Li, J. W. Lynn, J. L. Zarestky, and D. Vaknin Phys. Rev. B **78**, 184429 (2008).
- [21] J. Li, W. Tian, Y. Chen, J. L. Zarestky, J. W. Lynn, and D. Vaknin, Phys. Rev. B **79**, 144410 (2009).
- [22] J. Li, and D. Vaknin (unpublished results).
- [23] I. Abrahams K. S. Easson, Acta Crystallogr. Sect. C **49**, 925 (1993).
- [24] J. M. Mays, Phys. Rev. **131**, 38 (1963).
- [25] R. P. Santoro, D. J. Segal, and R. E. Newnham, J. Phys. Chem. Solids **27**, 1192 (1966).
- [26] R. P. Santoro and R. E. Newnham, Acta Crystallogr. **22**, 344 (1967).
- [27] T. B. S. Jensen, N. B. Christensen, M. Kenzelmann, H. M. Rønnow, C. Niedermayer, N. H. Andersen, K. Lefmann, J. Schefer, M. v. Zimmermann, J. Li, J. L. Zarestsky, and D. Vaknin, Phys. Rev. B **79**, 092412 (2009).
- [28] D. Vaknin, J. L. Zarestky, J. E. Ostenson, B. C. Chakoumakos, A. Goñi, P. J. Pagliuso, T. Rojo, and G. E. Barberis, Phys. Rev. B **60**, 1100 (1999).
- [29] D. Vaknin, J. L. Zarestky, L. L. Miller, J.-P. Rivera, and H. Schmid, Phys. Rev. B **65**, 224414 (2002).
- [30] M. Mericer, P. Bauer, C. R. Acad. Sci. Paris, **267**, 465 (1968).
- [31] M. Mercier, Ph.D. thesis, Universit de Grenoble, 1969.
- [32] J. P. Rivera, Ferroelectrics **161**, 147 (1994).
- [33] V. I. Fomin, V. P. Genezdilov, V. S. Kurnosov, A. V. Peschanskii, A. V. Yeremenko, H. Schmid, J. -P. Rivera, and S. Gentil, Low Temp. Phys. **28**, 203 (2002).
- [34] P. A. Lindgård, A. Kowalska, and P. Laut, J. Phys. Chem. Solids **28**, 1357 (1967).
- [35] J. L. Zarestky, D. Vaknin, B. C. Chakoumakos, T. Rojo, A. Goñi, and G. E. Barberis, J. Magn. Mag. Mat. **234**, 401 (2001).
- [36] N. B. Ivanov, Phys. Rev. B **47**, 9105 (1993).
- [37] B.-G. Liu, F.-C. Pu., G. Czycholl, J. Magnes. Mag. Mater. **154**, 369 (1996).